THE EUROPEAN
PHYSICAL JOURNAL
SPECIAL TOPICS

Regular Article

Convection effect on solidification microstructure: dendritic arm spacing and microsegregation

P. K. Galenko[1,2,a]

[1] Department of Theoretical and Mathematical Physics, Laboratory of Multi-Scale Mathematical Modeling, Ural Federal University, 620000 Ekaterinburg, Russia
[2] Faculty of Physics and Astronomy, Friedrich-Schiller-Universität-Jena, Otto Schott Institute of Materials Research, 07743 Jena, Germany

Abstract Convection affect primary crystalline structure, particularly, the dendrite crystal velocity and dendrite tip radius. The present work aims on the influence of the convective flow on the primary dendrite spacing between neighbouring crystals within the dendrite ensemble. Solidification of a binary alloy is considered within the model of stagnant boundary layer, under imposed thermal gradient which influence on the crystal microstructure and chemical microsegregation. Chemical composition in the solidifying liquid and crystalline solid is derived from the solution of the solute diffusion transport equation taking into account the convective flow. The model results are consistent with the Scheil-Brody-Flemings model, experimental data and computational results.

1 Introduction

The growth kinetics of crystals and their morphology depend on the properties of the crystal-liquid interface, the intensity of heat and solute transport around the interface, and the influence of external fields [1]. The theoretical description of these effects makes it possible to interpret the experimental data and predict the modes of crystal growth [2, 3]. Special attention is paid to the influence of the Earth's gravitational field on the occurrence of convective flows in the sample under study and the influence of hydrodynamic field on the kinetics of crystal growth [4–7].

Even if a special attention is usually paid to the effect of convection on the growth of a single dendrite [8–11], many theoretical aspects of the effect of convection on the structure formation of crystals and defect formation are not available in the literature. In particular, the dendrite arm spacing is available in the literature [12], however, an influence of convection on the distance between dendrites and, especially, on chemical microheterogeneity has not been qualitatively and quantitatively described theoretically.

[a] e-mail: peter.galenko@uni-jena.de (corresponding author)

The chemical microheterogeneity exhibits as chemical (inter)dendritic microsegregation which will be simply called in the present work as "microsegregation". Therefore, the main goal of this work is to present one of theoretical descriptions on the formation of an ensemble of crystalline microstructure which is influenced the convective flows.

2 Types of convection in solidification

The intensity of nucleation and growth, as well as the shape of crystal microstructures, directly depends on the conditions of heat and mass transfer at the solid–liquid interface. If the usual conductive transfer conditions are added also by the convective transfer due to the movement of the liquid phase, this can radically change the microstructure of the metal and alloy.

The effect of convective flow on the growth of crystals leads to the change of heat and mass transfer from the solid–liquid interface [13]. Such a change in the interface kinetics affects the growth velocity, the shape of the crystals, and may cause the change of the whole rate of sample solidification. These changes depend of the liquid flow intensity which is influenced by (i) density differences between phases, (ii) density gradients as a consequence of temperature gradients and/or variations in impurity concentration (buoyancy), (iii) surface tension gradients or (iv) externally introduced effects

1262

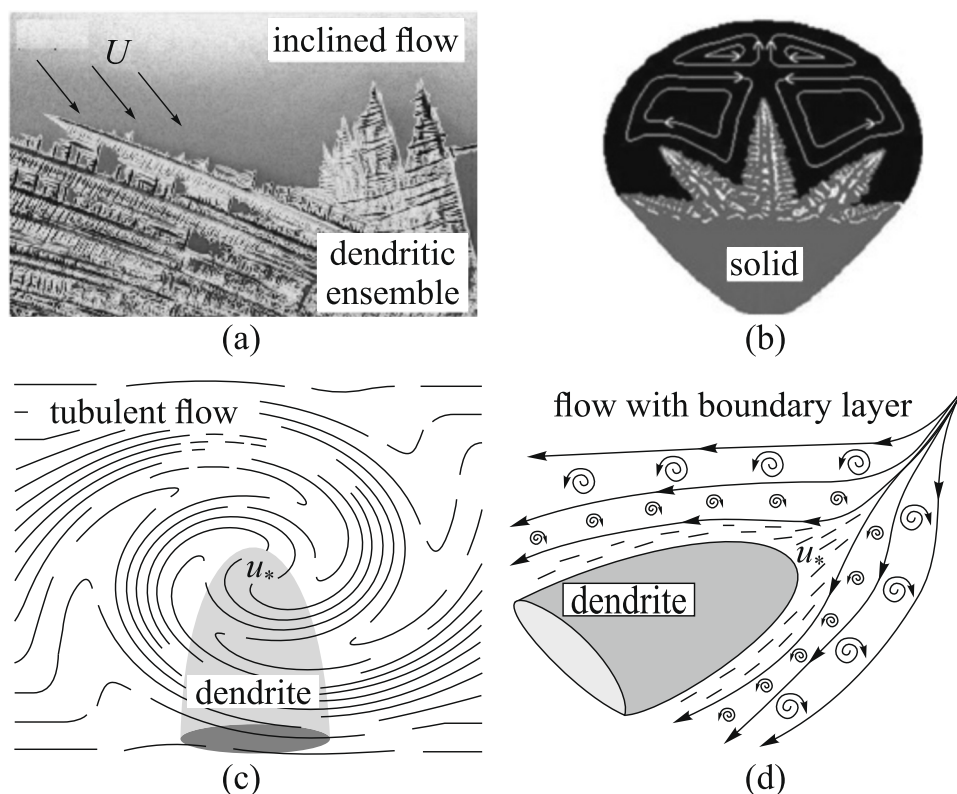Eur. Phys. J. Spec. Top. (2023) 232:1261–1271

Fig. 1 Various types of convection with various orientations of growing dendrites: **a** the flow inclined to the growth direction of the main stems of dendrites [14]; **b** the flow induced by the alternating electromagnetic field leading to the flow's cells in two spatial dimensions and to two torus in the three dimensional case [15]; **c** the liquid curl which covers the whole dendrite due to the intensive turbulent-nonstationary flow (here u_* means the friction velocity, in other words, the velocity with which the intense flow may press the dendrite) [10, 26]; **d** the flow with a number of small liquid curls providing however the hydrodynamic layer with laminar flow or even stagnant thermo-solute transport layer around the steady growing dendrite tip

such as electromagnetic stirring and sample deformation. Noticeable fluid flow may also be caused by moving solid phases due to sedimentation of grains or front shifting during continuous casting [16, 17]. As a result, various convection types in solidifying metals, metalloids, semiconductors and alloys are systematized as:

- forced convection induced by external fields such as gravitational, electro-magnetic or vibrational fields,

- Marangoni convection appearing due to gradients of surface energy,

- convection induced by the Soret effect existing by different diffusion ability of species in a chemically binary liquid,

- natural convection due to difference in density of the warm and cold parts of a sample.

These convective flows provide turbulent or laminar motion of liquid within the various ranges of crystal growth modes (chemically-solutal, thermo-solutal, thermal, or kinetically controlled regimes [18, 19]). A few examples of convective flows with the dendritic pattern are summarized in Fig. 1.

Number of various types of convection and crystal formation modes makes the analysis of their effect on

the solid phase formation quite complicated in a general case. To demonstrate the effect of convection on microstructure formation, only one type of convection and only one mode of crystal growth as a limiting case can, for instance, be chosen. It suffices to evaluate the convection effect on two main parameters of the growth of a dendritic crystal - tip velocity V and its radius R.

3 The stagnant boundary layer

Consider natural convection in combination with thermo-solutal transport of heat and species in a binary alloy during dendrite crystal growth. An inclined flow, Fig. 1a, leads to a transitional regime of the dendrite rotation to the direction of the flow. Indeed, when the liquid flows at an angle to the dendrite axis, the dendrite growth direction tends to alter during growth to become opposite to the flow direction [20]. Therefore, we will consider the case of steady-state growth under liquid flow assumed to be axi-symmetric along the axis of the dendrite in a direction opposite to the
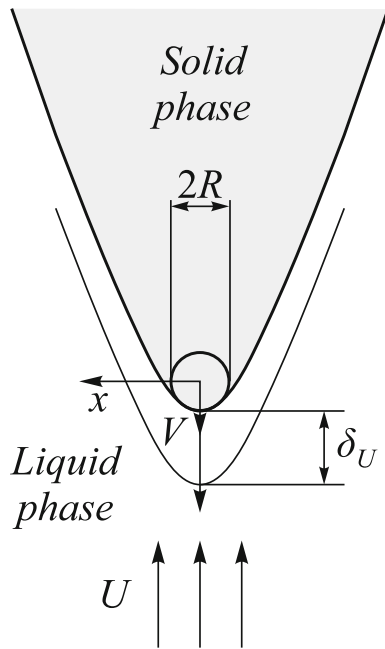
Eur. Phys. J. Spec. Top. (2023) 232:1261–1271

1263

Fig. 2 Scheme of the dendrite growing with the steady radius R, constant velocity V and the stagnant boundary layer δ_U, Eq. (1), around its surface

dendrite growth direction. Such consideration is likely to be applicable to a large number of practical cases.

Figure 2 demonstrates a well-developed dendrite particle growing along the z-axis within the Cartesian coordinate system. The incoming flow is parallel to the dendrite growth direction. The dendrite grows with the constant velocity V and steady tip radius R under buoyancy driven convection significantly influencing the tip velocities and the overall growth of a dendrite [21]. In metal-based alloys, such convection is driven by both thermal and solutal gradients in the melt and exists on earth and under low undercooling.

To estimate effect of convection, the approach based on the stagnant thermal and solutal boundary layer around the growing dendritic tip is used [24]. The effect of fluid flow is introduced by restricting the thermal and solute diffusion fields to a thin, stagnant boundary layer of the thickness δ_U. The boundary layer (see Fig. 1(d)) is produced by any additional fluid velocity U with the velocity-dependent thickness

$$\delta_\mathrm{U}/R = 2\mathrm{Re}^{1/2}, \tag{1}$$

where Re is the Reynolds number given in Table 1 summarising all other characteristic numbers necessary for comparative evaluation of the liquid flow and dendrite growth. Expression (1) appears in the dimensional analysis of the motion equations for fluid flow (Navier–Stokes equations) ignoring high order terms in the boundary layer thickness δ_U [24]. Using the definition of Re from Table 1, the boundary layer thickness is obtained by Eq. (1) as $\delta_\mathrm{U} \propto (\nu R/U)^{1/2}$. This expression explicitly shows that the stagnant boundary

layer around the dendrite tip increases with the increase of the kinematic liquid viscosity ν as well as with the larger dendrite tip radius R. By contrast, the boundary layer becomes thinner with the increase of the flow velocity U by the square root law.

The dendrite growth in alloy exists with a thermal boundary layer δ_T and a solute boundary layer δ_C, where the main intensive transport of heat and species occurs. When a liquid flows across the region of paraboloidal dendrite tip, these layers are related to a velocity (or momentum) boundary layer δ_U by the empirical laws [25]

$$\delta_\mathrm{T} = \delta_\mathrm{U}\mathrm{Pr}^{-1/3}, \quad \delta_\mathrm{C} = \delta_\mathrm{U}\mathrm{Sc}^{-1/3} \tag{2}$$

The Schmidt number, Sc, has larger values and the Prandtl number, Pr, is smaller than unity having typical values of the material parameters for liquid metals and alloys (see Table 1). Therefore, the stagnant boundary layer has a thickness in between the thickness for solute and thermal layers: $\delta_\mathrm{C} < \delta_\mathrm{U} < \delta_\mathrm{T}$. In the particular case of laminar thermosolutal natural convection, the boundary layers δ_T and δ_C ahead of the growing dendrite are given by [8, 27]

$$\frac{\delta_\mathrm{T}}{R} = 2.2\mathrm{Ra}_\mathrm{T}^{-1/4}\left(1 + \frac{\mathrm{N}}{\sqrt{\mathrm{Le}}}\right)^{-1/4}, \quad \frac{\delta_\mathrm{C}}{R}$$
$$= 2.2\mathrm{Ra}_\mathrm{C}^{-1/4}\left(1 + \frac{\sqrt{\mathrm{Le}}}{\mathrm{N}}\right)^{-1/4} \tag{3}$$

The main outcome following from the definitions of Table 1 and Eq. (3) reads as the increase of the Rayleigh numbers $\mathrm{Ra}_\mathrm{T,C}$ mainly with the increase of the undercooling $T_\mathrm{T}^* - T_0$ for Ra_T or saturation $C_\mathrm{T}^* - C_0$ for Ra_C makes the thickness of the thermal and solute layers thinner.

4 Modified Ivantsov solutions and selection criterion

When a dendrite grows with velocity V into a static (stagnant) melt, the bulk liquid has a relative velocity of V in the opposite direction with respect to the dendrite surface. Analytical solutions for the parabolic (paraboloidal) dendrite with the tip radius R are described by [22, 23]

$$\Omega_\mathrm{T;C} = P_\mathrm{T;C} \exp\left(P_\mathrm{T;C}\right)E_1(_\mathrm{T;C}) \tag{4}$$

for the supersaturation and undercooling Ω in three spatial dimensions and with the dimensionless thermal undercooling and supersaturation

$$\Omega_\mathrm{T} = \frac{T_\mathrm{T}^* - T_\infty}{\theta_\mathrm{T}}, \quad \Omega_\mathrm{C} = \frac{C_\mathrm{T}^* - C_\infty}{C_\mathrm{T}^*(1 - k)}, \tag{5}$$

Table 1 Characteristic numbers[a] of the dimensional analysis of the equations for fluid flow (Navier–Stokes) and conductive transport

Number	Expression	Values
Reynolds number, Re	UR/ν	$2 \cdot 10^{-8} - 10^{-6}$
Prandtl number, Pr	ν/a	0.13
Schmidt number, Sc	ν/D	$6 \cdot 10^2$
Lewis number, Le	a/D	$7.5 \cdot 10^3$
Thermal Rayleigh number, $\mathrm{Ra_T}$	$\dfrac{\beta_{\mathrm{Tg}}(T_{\mathrm{T}}^* - T_\infty)R^3}{a\nu}$	$2 \cdot 10^{-15}(T_{\mathrm{T}}^* - T_\infty)$, 1/K
Solutal Rayleigh number, $\mathrm{Ra_C}$	$\dfrac{\beta_{\mathrm{Cg}}(C_{\mathrm{T}}^* - C_\infty)R^3}{D\nu}$	$2 \cdot 10^{-9}(C_{\mathrm{T}}^* - C_\infty)$, 1/at.%
Buoyancy parameter, N	$\dfrac{\beta_{\mathrm{C}}(C_{\mathrm{T}}^* - C_\infty)}{\beta_{\mathrm{T}}(T_{\mathrm{T}}^* - T_\infty)} = \dfrac{\mathrm{Pr}}{\mathrm{Sc}}\dfrac{\mathrm{Ra_C}}{\mathrm{Ra_T}}$	$\dfrac{C_{\mathrm{T}}^* - C_\infty}{T_{\mathrm{T}}^* - T_\infty} \cdot 10^3$
Thermal Péclet number, P_{T}	$VR/(2a)$	$3.33 \cdot 10^{-3}V$ s/m
Solutal Péclet number, P_{C}	$VR/(2D)$	$16.67\,V$ s/m

[a]The characteristic numbers are estimated by the following values of material parameters: the liquid diffusion coefficient $D = 3 \cdot 10^{-9}$ m^2/s; the thermal diffusivity $a = 1.5 \cdot 10^{-5}$ m^2/s; the kinematic viscosity $\nu = 2 \cdot 10^{-6}$ m^2/s the dendrite tip radius $R = 10^{-7}$ m; solutal expansion coefficient $\beta_{\mathrm{C}} = 2 \cdot 10^{-2}$ 1/at.%; thermal expansion coefficient $\beta_{\mathrm{T}} = 2 \cdot 10^{-5}$ 1/K; gravity acceleration $g = 10$ m/s^2; velocity of the natural thermosolutal convection $U = 10^{-6} - 10^{-4}$ m/s

where T_{T}^* and C_{T}^* are the temperature and the concentration, respectively, at the dendrite tip, T_∞ and C_∞ are the temperature and concentration, respectively, far from the dendrite in the liquid.

The dendrite growing in the incoming axisymmetric flow with the formed stagnant boundary layer around its tip still have parabolic (paraboloidal) shape. The thermal and solute fields, however, are deformed due to flow. The thermal and solutal fields (4) in the presence of the stagnant boundary layer are expressed, therefore, by the modified Ivantsov solution [24]

$$\Omega_{\mathrm{T}} = P_{\mathrm{T}} \exp{(P_{\mathrm{T}})}\{E_1(P_{\mathrm{T}}) - E_1[P_{\mathrm{T}}(1 + 2(\delta_{\mathrm{T}})/R)]\}, \tag{6}$$

$$\Omega_{\mathrm{C}} = P_{\mathrm{C}} \exp{(P_{\mathrm{C}})}\{E_1(P_{\mathrm{C}}) - E_1[P_{\mathrm{C}}(1 + 2(\delta_{\mathrm{C}})/R)]\}. \tag{7}$$

As predicted by Eqs. (6) and (7), solutions for Ω_{T} and Ω_{C} are proportional to the difference, $E_1(P_{\mathrm{T,C}}) - E_1[P_{\mathrm{T,C}}(1 + 2\delta_{\mathrm{T,C}}/R)]$, between exponential integral functions of the first kind E_1. This difference appears due to introducing the stagnant boundary layer and indicates the decreasing of the dendrite tip temperature T_{T}^* and concentration C_{T}^* in the presence of liquid flow around the tip. With the increase of the boundary layer up to infinity, $\delta_{\mathrm{U}}/R \to \infty$, the thermal and solutal layers also abnormally increase, $\delta_{\mathrm{T}} \to \infty$ and $\delta_{\mathrm{C}} \to \infty$ by the empirical expressions (2). Second exponential integral functions in the right-hand sides of Eqs. (6) and (7) transform to zero, $[P_{\mathrm{T,C}}(1 + 2\delta_{\mathrm{T,C}}/R)] \to E_1[\infty] \to 0$, and one gets the Ivantsov solution (4) for the conductive transport without convective motion of the liquid.

In the limit of high dendrite velocity V, the drastic decreasing the solute boundary layer occurs: $\delta_{\mathrm{C}} \to 0$.

In this limit, the difference between exponential integral functions in Eqs. (6) and (7) approaches zero: $\Omega_{\mathrm{C}} \propto E_1(P_{\mathrm{C}}) - E_1[P_{\mathrm{C}}(1 + 2\delta_{\mathrm{C}}/R)] \to 0$. Then the supersaturation (5) shows clear tendency to the chemically partitionless dendrite growth: the dendrite tip concentration tends to the initial (nominal) composition $C_{\mathrm{T}}^* \to C_\infty$ as $\delta_{\mathrm{C}} \to 0$.

Thermal undercooling and supersaturation (6) and (5) modify the undercooling balance $\Delta T = \Delta T_{\mathrm{T}} + \Delta T_{\mathrm{C}} + \Delta T_{\mathrm{R}}$ as

$$\Delta T = \theta_{\mathrm{T}}\Omega_{\mathrm{T}} + \frac{k\Delta T_0\Omega_{\mathrm{C}}}{1 - (1 - k)\Omega_{\mathrm{C}}} + 2\Gamma/R. \tag{8}$$

This balance predicts the dendrite tip velocity V and tip radius R for a given bulk undercooling ΔT. To obtain V and R separately, one should also use the second equation which is given by the selection criterion for the stable dendrite growth. The criterion is re-written as

$$\sigma^* = \Gamma/R[\theta_{\mathrm{T}}P_{\mathrm{T}} + 2P_{\mathrm{C}}(k\Delta T_0)/(1 - (1 - k)\Omega_{\mathrm{C}})]^{-1} \tag{9}$$

with σ^* the selection parameter independent of the undercooling, alloy composition, and flow velocity in the zero approximation of the dendrite growth model [13].

Two equations (8) and (9) describe two main parameters of the primary dendrite crystallization, namely, the dendrite tip velocity V and tip radius R for a given undercooling ΔT. The undercooling balance (8) is influenced by convective flow through the functions (6) and (7). The selection criterion (9) was derived in

Fig. 3 Comparison of measured and predicted dendrite tip velocities V (**a**) and tip radii R (**b**) as a function of undercooling ΔT in the succinonitrile-0.1045 wt% acetone melt. The predictions were made using Eqs. (8) and (9) with and without convective flow [9]
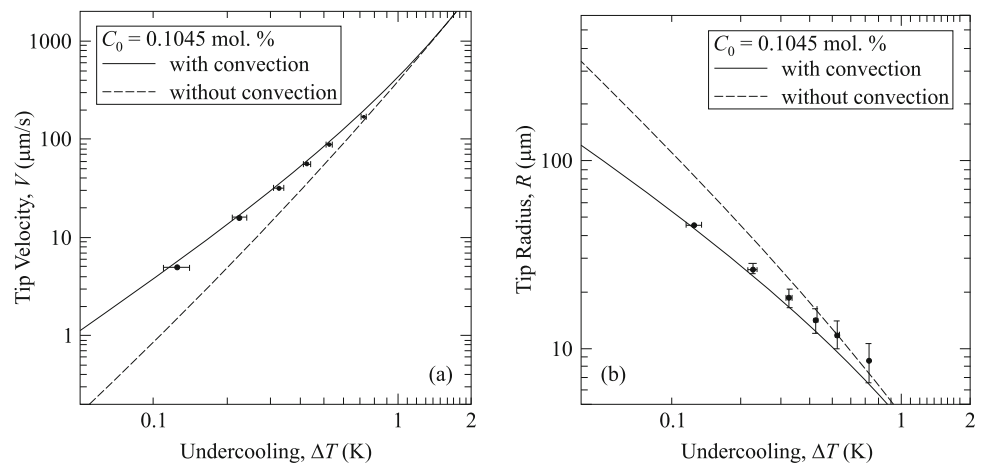
the limit of stagnant liquid phase. To be consistent, Eq. (9) should also include effect of the flow on the selection of the stable dendrite growth mode [13, 19]. Therefore, the existing model of boundary layer can be extended using the convective terms in the selection criterion of the dendrite growth.

5 Comparison with experiment

Simultaneous solution of the equations for balance (8) and criterion (9) provide the obtaining dendrite velocity $V(\Delta T)$ and its tip radius $R(\Delta T)$ for a given bulk undercooling ΔT, the chosen value of the selection parameter σ^* and with calculated numbers from Table 1. Figure 3 presents the solution of Eqs. (8) and (9) for the dendrite growth in the succinonitrile $-$ 0.145 mole% acetone melt under thermosolutal convection [9]. The dendrite tip velocity (Fig. 3a) and its radius (Fig. 3b) are obtained with the value of selection parameter σ^* =0.02.

The solution of Eqs. (8) and (9) is given for the finite values of the thermal δ_T and solutal δ_C layers in the presence of convective flow (solid lines). For the infinite values of thickness $\delta_\text{T} \rightarrow \infty$ and $\delta_\text{C} \rightarrow \infty$ the solution is shown by the dashed lines, i.e. when the convection is absent and the dendrite is growing in the stagnant melt. As expected, the tip velocity increases (Fig. 3a) and the tip radius decreases (see Fig. 3b) as the undercooling increases. Moreover, the "convective branch" (solid curve) shows the increasing the velocity and decreasing tip radius in comparison with their "stagnant, non-convective branch" (dashed curve). In this behavior, the role of the flow is completely pronounced: the flow increases the crystal growth velocity and makes the dendrite trunks and their axes thinner.

Shown in Fig. 3, the solutions for the dendrite velocity V and dendrite tip radius R demonstrate excellent agreement with experimental data on dendrite growth from succinonitrile-acetone melt. In the range of smallest undercooling $\Delta T < 0.5$ K, the dendrite growth proceeds along the "convective branch": V and R are described well by the solid lines of their behavior. As

Fig. 3 also shows, V and R transfer from the "convective branch" (solid curves) to the "stagnant non-convective branch" (dashed curves) of their behavior in the range of the higher undercooling $\Delta T > 0.5$ K. Such change of the behavior occurs because the dendrite growth velocity essentially overcomes the fluid flow velocity at larger undercooling and the dendrite becomes insensitive to the influence of convective flow.

The obtained influence of the convective flow on the dendrite growth in example of thermosolutal natural convection is the universal effect. For instance, the increase of the velocity and thinning of dendrites is found also in the presence of forced convection [28]. The phase field modelling with the convective flow also shows pronounced increasing of the dendrite growth velocity for dendrite growing in the direction opposite to the flow [29]. As Fig. 4 shows, the results of phase field modelling predict the velocity increase for the downward trunk growing towards the incoming stream shown by the small arrows (which characterize the vector flow velocities along the stream-lines of the flow). For the undercooling $\Delta T = 0.55\theta_\text{T}$ and incoming flow velocity $U = 0.07 D_\text{T} \theta_\text{T}/\Gamma$, Fig. 4a-c demonstrates the pronounced evolution of the dendrite trunk growing in the opposite direction to the liquid flow. This tendency remains the same for three spatial dimensions, Fig. 5.

6 Influence of the convection on the microstructure

6.1 Primary dendritic spacing

Effect of convection on the primary dendritic (or cellular) spacing can be demonstrated for the constrained growth of crystals. This type of directional solidification is characterized by the constant thermal gradient G under which the solute diffusion and convection of species play the main role in the formation of the distance λ_1 between trunks (main stems) of dendrites (see Fig. 6).

1266

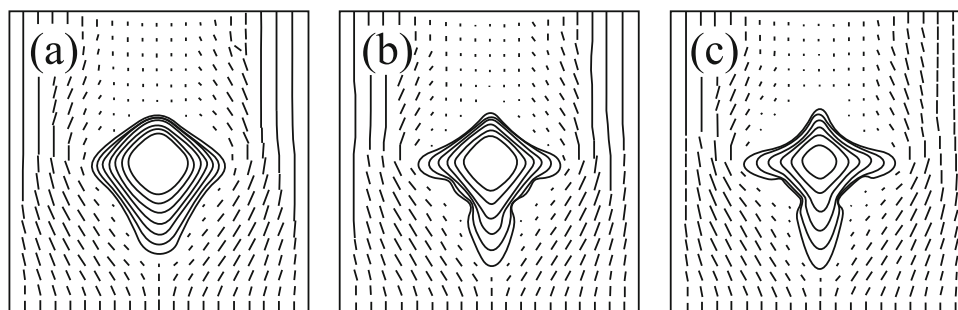Eur. Phys. J. Spec. Top. (2023) 232:1261–1271

Fig. 4 Influence of incoming two-dimensional flow on nickel dendrite growth [29]. An evolution of phase-field contours is shown for a dendrite growing from undercooled nickel melt if the incoming flow is directed from bottom to top of domain. Dashed lines around crystals show the relative values and direction of the flow velocity. The difference in the dendrite morphology from (**a**) to (**c**) is provided by various values in the computationally imposed anisotropy of the solid–liquid interface energy in $\langle 10 \rangle$- and $\langle 11 \rangle$-directions of two-dimensional growth. Quantitatively, the anisotropy is given by the ε-parameter as: **a** $\varepsilon = 0.01$, **b** $\varepsilon = 0.03$, and **c** $\varepsilon = 0.05$
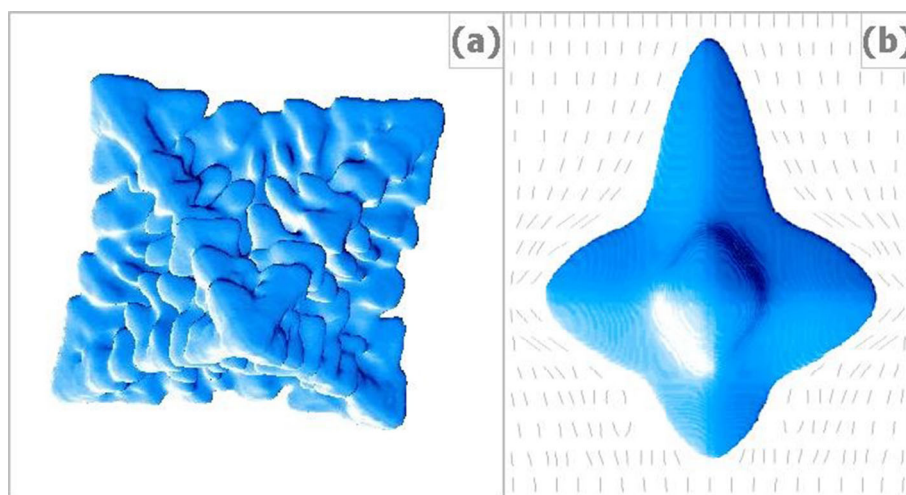
Fig. 5 Influence of incoming three-dimensional flow on nickel dendrite growth modelled by the phase field method. **a** Dendrite growing symmetrically into pure nickel undercooled at $\Delta T = 0.55 \theta_T$ K. Pattern has been simulated on a grid of size 6503 nodes [30]. **b** Growth of nickel dendrite under convective flow at $\Delta T = 0.30 \theta_T$ K and $U = 0.7$ m/s. The direction of the incoming flow is from top to bottom of computational domain that is shown by dashed lines. Growth velocity of the up-stream branch is pronounced in comparison with the down-stream branch due to forced convection. Dashed lines around the dendrite indicate the flow velocity vectors in the vertical cross-section. Pattern has been simulated on a grid of size $230 \times 230 \times 330$ nodes [31]

Assume that the directionally growing dendrites have the same tip radii R. Then, the primary dendritic spacing is given by expression (A9.40) from the book [32]

$$\lambda_1 = \left(\frac{3 \Delta T' R}{G} \right)^{1/2} \qquad (10)$$

In this expression, R is obtained from Eq. (9), $\Delta T' = m(1 - k) C_T^*$ is the non-equilibrium solidification interval. Neglecting the thermal contribution, this yields

$$R = \left(\frac{\Gamma D}{\sigma^*} \cdot \frac{1 - (1 - k)\Omega_C}{kV \Delta T'} \right)^{1/2} \qquad (11)$$

In this expression, supersaturation Ω_C is defined by the modified Ivantsov solution (7) dependent on the conductive diffusion transport (4) and the contribution $E_1[P_C(1 + 2(\delta_C)/R)]$ due to the introducing solute boundary layer δ_C. The latter directly depends on the stagnant boundary layer δ_U, Eqs. (1)–(2), formed by the convective liquid flow. In this connection, the primary dendritic spacing (11) is influenced by convection.

Substituting dendrite tip radius (11) into the expression (10) gives the dependence of primary spacing on both the diffusion conductive and convective solute transport

$$\lambda_1 = \left(\frac{3}{G} \right)^{1/2} \left(\frac{\Gamma D \Delta T'}{\sigma^* kV} [1 - (1 - k)\Omega_C(P_C, \delta_C/R)] \right)^{1/4}. \qquad (12)$$

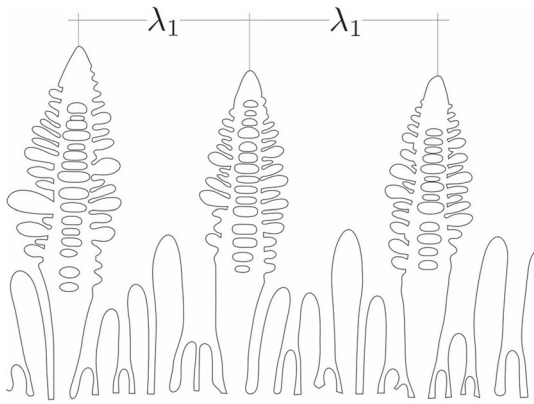Eur. Phys. J. Spec. Top. (2023) 232:1261–1271

1267

Fig. 6 Dendritic crystals formed after morphological instability of the planar solid–liquid interface and the further selective process among crystals during directional solidification. The temperature gradient is directed from bottom to top along the dendritic stems. The average distance between dendrites, i.e. the dendrite arm spacing λ_1, is shown in the regime of quasi-stationary growth of selected crystals at the constant velocity V
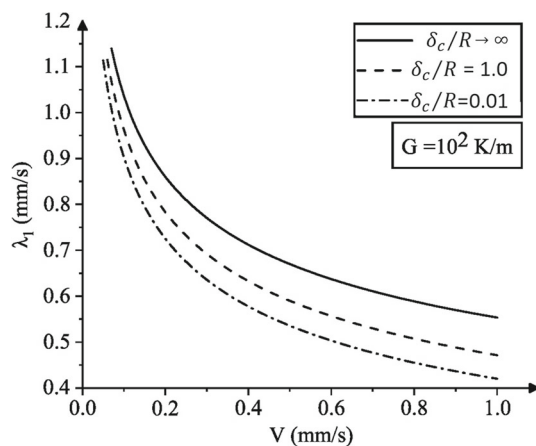
Fig. 7 Dependence of the primary dendritic spacing λ_1 on the dendrite tip velocity V. Different values of the ratio δ_C/R present different influence of the convective velocity U by Eqs. (1)-(3)

Expression (12) extends the discussed approaches on the primary dendrite arm spacing [12] by taking the convective flow into account. Under the condition of solute diffusion transport only, $\delta_C/R \to \infty$, and, therefore, due to negligible Ivantsov function (4), $\Omega_C = P_C \exp(P_{T;C}) E_1(\infty) \to 0$, Eq. (12) transforms into expression (A9.41) of the book "Fundamentals of Solidification" by Kurz and Fisher [32].

The whole solution of the primary trunk spacing λ_1 by Eq. (12) is shown in Fig. 7 for three cases of convective transport. Namely, the solid curve with $\delta_C/R \to \infty$ shows λ_1 in the flow absence, the behavior of dashed curve predicts λ_1 under moderate convective transport with $\delta_C/R = 1$, and, finally, the case $\delta_C/R = 0.01$ drawn by the dashed-dotted curve exhibits λ_1 formed

under influence of intensive natural convection. These curves are given as functions of the dendrite growth velocity V with the taken constant thermal gradient $G = 100$ K/m. All other material parameters are taken for Al-2wt%Cu from the book [32]. As is clearly seen in Fig. 7, the primary spacing λ_1 decreases with the increase of the dendrite tip velocity V and for the increase of the flow intensity at a given value of V. A similar tendency towards thinning of the microstructure accompanied by a decrease in the parameter λ_1 is observed with an increase in the temperature gradient G under fixed convection intensity (i.e., with fixed ratio δ_C/R. The distance between primary dendrite trunks decreases as the temperature gradient G becomes larger according to the square root law of Eq. (12).

6.2 Microsegregation

The effect of the liquid flow on the chemical segregation of the interdendritic space (microsegregation) is analysed here within the framework of the Scheil-Brody-Flemings-type model [33, 34]. Such a microsegregation model predicts influence of the flow on the non-equilibrium impurity distribution in the interdendritic space and inside the primary dendrites. This makes it possible to estimate the accumulation of impurities also at the macrolevel, predicting a smooth increase (decrease) in the impurity along the growth directions of crystals from the beginning to the end of solidification process.

Consider the diffusion-convection transport within heterogeneous mushy zone during binary alloy solidification [35–37]. For simplicity, further analysis is given in one-dimensional space where diffusion and convection proceed along the z-axis, which co-insides with the direction of crystals' growth. The change of the liquid concentration C_L in the solidifying mushy zone is described by
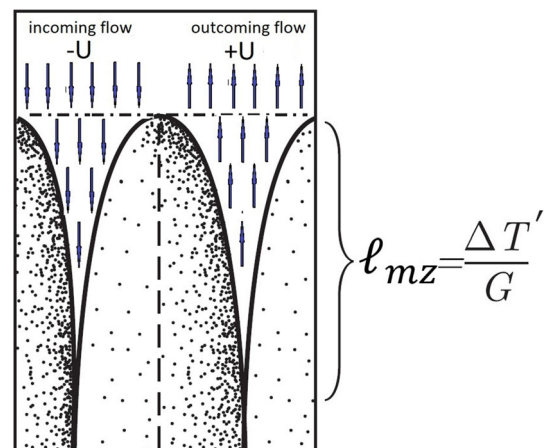

Fig. 8 Scheme of dendritic array with upcoming and outgoing liquid flow. Here: $\Delta T'$ is the non-equilibrium temperature interval of solidification and G is the thermal gradient within the two-phase mushy zone

$$(1 - f_S)\frac{\partial C_L}{\partial t} + (1 - f_S)U\frac{\partial C_L}{\partial z}$$
$$= \frac{\partial}{\partial z}\left[(1 - f_S)D_L\frac{\partial C_L}{\partial z}\right] - 2\alpha f_S k\frac{\partial C_L}{\partial t} + (1 - k)C_L\frac{\partial f_S}{\partial t}, \tag{13}$$

where f_S is the solid fraction at a given point of coordinate z at the time t and U is the averaged velocity of the flow. The first term in the left-hand side of Eq. (13) describes the change of the liquid concentration in time at the considered point of mushy zone with the liquid fraction $1 - f_S$. The second term in the left-hand side of Eq. (13) takes the change of spatial distribution of concentration into account due to the liquid flow having the velocity U. Note that

- the influence of the flow decreases with the increasing of the solid fraction due to the contribution $(1 - f_S)U$;

- the stream can be opposite to the growth direction of crystals, therefore, the flow velocity takes negative value, i.e. $U < 0$, for so called "incoming flow into interdendritic space" (as is shown in left part of Fig. 8);

- the stream can have the same direction as crystals' growth, therefore, the flow velocity takes positive value, i.e. $U > 0$, for so-called "outcoming flow from the interdendritic space" (as is shown in right part of Fig. 8).

The first term in the right-hand side of Eq. (13) describes the solute diffusion with the coefficient $(1 - f_S)D_l\partial C_L/\partial z$ and the second term predicts the transport of the solute into the solid phase in which the concentration changes as $C_S = kC_L$. The factor 2α takes the solid-state back-diffusion, see Appendix 12 in book [32]. Finally, the last term in the right-hand-side of Eq. (13) predicts the intensity of the precipitation of solid phase evolving in time. This last term plays a role of the source term for concentration in the diffusion-convective equation.

As in the approach of Scheil-Brody-Flemings [33, 34], one neglects the diffusion in liquid, $D_L = 0$. Then, using full differentials instead of partial derivatives, Eq. (13) takes the following form

$$(1 - f_S)dC_L + (1 - f_S)U\left(\frac{dz}{dt}\right)^{1/2}dC_L$$
$$+ 2\alpha f_S k dC_L = (1 - k)C_L df_S. \tag{14}$$

The remarkable factor dz/dt of the second term in the right-hand side of Eq. (14) represents the change of flow's coordinate with time might be evaluated as follows. The change in the liquid concentration, dC_L, proceeds due to the flow, $(1 - f_S)U$, along the z-axis of crystals' growth, Fig. 8. As such, the characteristic change of liquid flow within interdendritic space occurs in the distance $dz \approx \Delta z = \Delta T'/G$ defined by the nonequilibrium solidification range $\Delta T'$ and temperature gradient G existing in the scale of solidifying region. If the liquid phase has the kinematic viscosity, ν, then the liquid penetrates within the interdendritic space during the time $dt \approx \Delta t = (\Delta T'/G)^2/\nu$. Therefore, the factor of the second term in the right-hand side of Eq. (14) is

estimated as $(dz/dt)^{-1} \approx (\Delta T'/G)/\nu$. Combining this factor with the convection velocity U defines the ratio

$$U(dz/dt)^{-1} = \ell_{MZ}/\ell_U \tag{15}$$

between two characteristic length scales

$$\ell_U = \nu/U, \quad \ell_{MZ} = \Delta T'/G \tag{16}$$

The scale ℓ_U defines the characteristic length for the viscous liquid to flow within interdendritic space. As before, the scale ℓ_{MZ} defines the characteristic length of the interdendritic space, see Fig. 8). The ratio ℓ_{MZ}/ℓ_U estimates how deep the flow may penetrate effectively into the interdendritic space. Namely, if $\ell_{MZ} = 0.5\ell_U$, then only a half of the distance of the interdendritic space might be effectively accessible for the liquid flow.

Substitution of the ratio Eq. (15) into the governing equation Eq. (14) gives

$$\frac{dC_L}{(1 - k)C_L} = \frac{df_S}{(1 - f_S)(1 + \ell_{MZ}/\ell_U) + 2\alpha f_S k}. \tag{17}$$

Integration of Eq. (17) within interdendritic space

$$\frac{1}{(1 - k)}\int_{C_0}^{C_L}\frac{dC_L}{C_L} = \int_0^{f_s}\frac{df_S}{1 + \ell_{MZ}/\ell_U - (1 + \ell_{MZ}/\ell_U - 2\alpha k)f_s} \tag{18}$$

defines the final solution of Eq. (14) as

$$C_L = C_0\left[1 - f_S\left(1 - \frac{2\alpha k}{1 + \ell_{MZ}/\ell_U}\right)\right]^{\frac{k-1}{1 + \ell_{MZ}/\ell_U - 2\alpha k}} \tag{19}$$

The solution (19) describes nonequilibrium distribution of concentration in the liquid, C_L, and solid, $C_S = kC_L$. This distribution is a function of solid phase fraction, f_S, and influenced by effects of liquid flow with $U \neq 0$ and solid-state back-diffusion at $\alpha \neq 0$. If the liquid moves in the direction opposite to the direction of dendritic growth, one has $U < 0$ and $\ell_{MZ}/\ell_U < 0$ due to Eq. (16). The liquid stream flows along the dendrites' growth direction with $U > 0$ and $U < 0$ giving the sign for the ratio ℓ_{MZ}/ℓ_U by Eq. (16). Both of theses cases are shown in Fig. 8).

In the absence of flow, $U = 0$, one has $\ell_U \to \infty$ by Eq. (16) leading to the vanishing ratio $\ell_{MZ}/\ell_U \to 0$ accordingly Eq. (15). The solution (19) arrives in this case at the solution of Brody and Flemings [34] $C_L = C_0[1 - f_S(1 - 2\alpha k)]^{(k-1)/(1-2\alpha k)}$ from which the solutions of Scheil [33] and equilibrium level rule with $\alpha = 0$ and $\alpha = 0.5$, respectively, are directly follow.

The solution (19) is plotted in Fig. 9 with $\alpha = 0.03$, $\ell_{MZ}/\ell_U = \pm 0.2$ and $k = 0.14$ for Al-2wt%Cu. For the stagnant interdendritic melt, $U = 0$ and $\ell_{MZ}/\ell_U = $
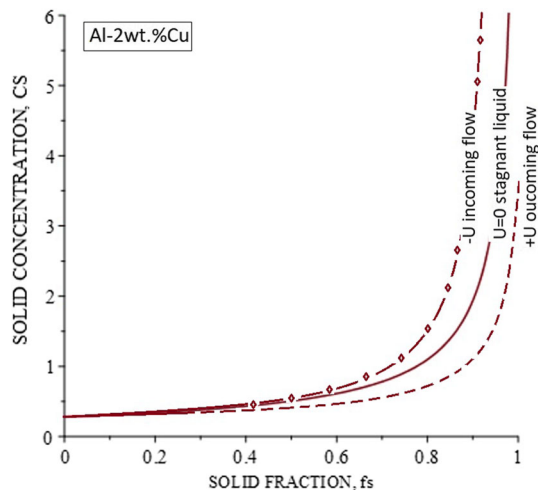
Fig. 9 Solid concentration $C_S = kC_L$ in the Al-2wt%Cu alloy calculated by the solution (19) with $\alpha = 0.03$. The convective flow is taken by the ratio of the length scale of mushy zone ℓ_{MZ} and the length scale of convection ℓ_U into account. The incoming flow is modelled by $\ell_{MZ}/\ell_U = -0.2$ (the direction of liquid flow is opposite to the direction of dendritic growth, $U < 0$) as well as the outcoming flow is modelled by $\ell_{MZ}/\ell_U = 0.2$ (the liquid flows in the direction of dendritic growth, $U > 0$) due to Eq. (16). The stagnant liquid if modelled by $U = 0$ giving the limit $\ell_{MZ}/\ell_U \to \infty$ and leading to the Brody-Flemings model. For computations, $C_0 = 2wt\%$ and $k = 0.14$ were taken from the book [32]

0, the solid concentration is predicted by the Brody-Flemings model [34] (see solid curve in Fig. 9. The incoming flow into interdendritic space, $U < 0$, is modeled by the parameter $\ell_{MZ}/\ell_U = -0.2$ that is shown by the dashed-dotted curve in Fig. 9). In this case, the concentration of copper in dendritic arms and trunks becomes higher than it is predicted by the Brody-Flemings model [34], especially, for the solid fraction $f_S \geq 0.5$. This occurs due to accumulation of copper by the incoming flow which brings additional quantity of copper to interdendritic space with the stream. Finally, the flow outcoming from the interdendritic space is given by the dashed curve in Fig. 9) calculated by Eq. (19) for $U > 0$ and with the ratio $\ell_{MZ}/\ell_U = 0.2$. It is seen that the outcoming flow decreases the copper concentration in the solid phase in comparison with the prediction of the Brody-Fleming model [34]. This fact naturally follows from the possibility of carrying the copper away from the interdendritic fluid due to the outgoing convective motion of the melt. As a result, the branches and trunks of the dendrites are copper-depleted in comparison to the prediction of the Brody-Flemings model [34].

The incoming flow considered in the present analysis is analogous to the downward flow in natural convection as well as outcoming flow imitates the upward flow in the natural convection. Therefore, the present analytical result and calculations shown in Fig. 9 are consistent with the results on phase field modeling of dendritic growth with solutal buoyancy [38]:

(a) the solute is confined to the interdendritic region due to downward flow, the concentration becomes higher inside dendrites and within interdendritic spacing;

(b) solute is transported out of the interdendritic regions with decreasing microsegregation due to existing upward flow.

The upward and downward liquid flows are of fundamental importance in the analysis of the morphological stability of solidification fronts [39]. In the case of the upward flow (flows out of the two-phase zone, flows out from the crystal), the crystal-liquid interface is always morphologically unstable that forms dendrites, cells and other crystalline structures. In the case of downward flow (flows into the two-phase zone, flows onto the crystal), both interface stability and its instability with the formation and development of dendrites (cells) are possible.

Note that in the solution of Eq. (13), it is assumed that a constant velocity U of the flow is set as a parameter. However, the problem can be solved consistently with the variable fluid flow in a two-phase mushy zone. Indeed, the flow velocity in the liquid core is defined by the Navier–Stokes equation which might be solved in a chosen approximation analytically or numerically [40]. The alternating flow velocity within the two-phase mushy zone can be estaimated by the Darcy's law [36]. In this case, the coupling of the diffusion-convective equation (13) with the Darcy's law leads to the self-consistent finding of concentration and flow velocity within the two-phase mushy zone.

Finally, interdendritic flow may influence the final morphology of the dendritic structure. Specifically, intensity and direction of flow may have am essential effect on the fragmentation of dendritic branches and even their trunks due to the change of interdendritic concentration within the mushy zone of solidifying alloy. Thus, the model presented in this article describes the effect of flow on microsegregation and the reverse effect of microsegregation on flow with a possible change in the shape of dendritic crystals.

7 Conclusions

In the present work, features of the crystalline microstructure formation in a binary alloy have been considered for solidifying melt under the influence of the liquid convective flow. The main result obtained in the work is the solution of the convective-diffusion equation for the incoming convective flow into the two-phase zone and the outcoming flow from it. This solution allows us to quantitatively estimate chemical microsegregation in two phase mushy zone and primary dendrite arm spacing as a distance between neighbouring stems of crystals depending on the flow intensity. The obtained particular results can be summarized as follows.

First, the model of stagnant boundary layer [24] for heat- and mass-transport has been analyzed. A thickness δ_U of the stagnant boundary layer depends on the

1270

Eur. Phys. J. Spec. Top. (2023) 232:1261–1271

flow velocity U as $\delta_{\mathrm{U}} \propto U^{-1/2}$. Because the solute boundary layer is proportional analytically to the stagnant boundary layer, $\delta_{\mathrm{C}} \propto \delta_{\mathrm{U}}$, the microstructure characteristics, especially, the distance between primary stems of dendrites, λ_1, also depends on the liquid flow intensity. This non-linear dependence expressed in the fact that the characteristic distance λ_1 decreases, i.e. the dendritic phase becomes much denser with the increase of the flow velocity U at the chosen constant value of the temperature gradient G inside the two phase mushy zone of directionally solidifying binary melt.

Second, the chemical microsegregation affected by the convective flow has been investigated analytically. Using the solution of the convective-diffusion transport equation an effect of the incoming flow and outcoming flow on chemical microsegregation inside two phase mushy zone has been established. The solute component is collected within the interdendritic region due to incoming flow, playing a role of a downward flow during buoyancy convective mechanism of flow, to the mushy zone. As the result, the concentration becomes higher inside dendrites and within interdendritic spacing. Contrary to this, the solute is transported out the interdendritic regions with the decrease of chemical microsegregation inside the two phase mushy zone due to existing outcoming flow, playing (which a role of an upward flow during buoyancy convective mechanism of flow.

Third, the forced convection induced by external fields has influence of the microstructure formation of solidifying metals and alloys. One can recollect that

- the static magnetic field imposed on the solidifying sample under different directions drastically influences on the dendrite growth kinetics [26, 41] and formation of defects [42, 43];
- convection may essentially influence on the formation of freckle, solute plume and dendritic fragmentation [44, 45] as well as on the Columnar-Equiaxed-Transition in crystalline structure [46].

Therefore, application of the present approach to the problem of microstructure formation under forced flow can be seen as a future perspective work.

Data Availability No Data associated in the manuscript.

Declarations

Conflict of interest The author declare no conflict of interests.

References

1. D.M. Herlach, D.M. Matson (eds.), *Solidification of Containerless Undercooled Melts* (Wiley-VCH, Weinheim, 2012)
2. W. Kurz, D.J. Fisher, R. Trivedi, Intern. Mater. Rev. **64**(6), 311 (2019)
3. P.K. Galenko, D.V. Alexandrov, Philos. Trans. R. Soc. A **376**, 20170210 (2018)
4. Ph. Bouissou, P. Pelcé, Phys. Rev. A **40**, 6673 (1989)
5. C. Beckermann, H.-J. Diepers, I. Steinbach, A. Karma, X. Tong, J. Comp. Phys. **154**, 468 (1999)
6. D.V. Alexandrov, P.K. Galenko, Phys. Rev. E **87**, 062403 (2013)
7. M. von Kurnatowski, K. Kassner, J. Phys. A Math. Theor. **47**, 325202 (2014)
8. Q. Li, C. Beckermann, J. Cryst. Growth **236**, 482 (2002)
9. A.J. Melendez, C. Beckermann, J. Cryst. Growth **340**, 175 (2012)
10. D.V. Alexandrov, P.K. Galenko, L.V. Toropova, Phil. Trans. R. Soc. A **376**, 20170215 (2018)
11. P.K. Galenko, D.A. Danilov, K. Reuther, D.V. Alexandrov, M. Rettenmayr, D.M. Herlach, J. Cryst. Growth **457**, 349 (2017)
12. J. Strickland, B. Nenchev, H. Dong, Crystals **10**(7), 627 (2020)
13. D.V. Alexandrov, P.K. Galenko, Philos. Trans. R. Soc. A **379**, 20200325 (2021)
14. N. Shevchenko, S. Boden, G. Gerbeth, S. Eckert, Metal. Mater. Trans. A **44A**, 3797 (2013)
15. O. Funke, G. Phanikumar, P.K. Galenko, L. Chernova, S. Reutzel, M. Kolbe, D.M. Herlach, J. Cryst. Growth **297**, 211 (2006)
16. C. Beckermann, J. Ni **23**(3), 315 (1996)
17. M. Wu, A. Ludwig, Acta Mater. **57**(19), 5621 (2009)
18. P.K. Galenko, D.A. Danilov, Phys. Lett. A **235**(3), 271 (1997)
19. D.V. Alexandrov, P.K. Galenko, Phys. Chem. Chem. Phys. **17**, 19149 (2015)
20. N. Shevchenko, O. Roshchupkina, O. Sokolova, S. Eckert, J. Cryst. Growth **417**, 1 (2015)
21. Y.W. Lee, R.N. Smith, M. Glicksman, M.B. Koss, Ann. Rev. Heat Transf. **7**, 59 (1997)

22. G.P. Ivantsov, Dokladi Academii Nauk USSR **58**, 567 (1947)
23. G.P. Ivantsov, Dokladi Academii Nauk USSR **83**, 573 (1952)
24. B. Cantor, A. Vogel, J. Cryst. Growth **41**, 109 (1977)
25. J.C. Brice, P. Rudolph, Crystal growth. In *Ullmann's Encyclopedia of Industrial Chemistry, Sixth Edition* (Wiley-VCH, Weinheim, 2002), pp. 1–83
26. J. Gao, A. Kao, V. Bojarevics, K. Pericleous, P.K. Galenko, D.V. Alexandrov, J. Cryst. Growth **471**, 66 (2017)
27. B. Gebhart, Y. Jaluria, R.L. Mahajan, B. Sammakia, *Buoyancy Induced Flows and Transport* (Hemisphere Publishing, New York, 1988)
28. S. Binder, P.K. Galenko, D.M. Herlach, J. Appl. Phys. **115**, 053511 (2014)
29. X. Tong, C. Beckermann, A. Karma, Phys. Rev. E **61**, R49 (2000)
30. B. Nestler, D.A. Danilov, P.K. Galenko, J. Comp. Phys. **207**, 221 (2005)
31. P.K. Galenko, G. Phanikumar, O. Funke. D.M. Herlach, in *Free Dendrite Growth in Undercooled Melt: Experiments and Modeling*. Solidification Processes and Microstructures Edited by TMS (The Minerals, Metals and Materials Society, 2004), pp. 277–288
32. W. Kurz, R. Fisher, *Fundamentals of Solidification* (Trans Tech, Aedermannsdorf, 1989)
33. E. Scheil, Z. Metallk. **34**, 70 (1942)
34. H.D. Brody, M.C. Flemings, Trans. TMS-AIME **236**(1), 615 (1966)
35. M.C. Flemings, G.E. Nereo, Trans. TMS-AIME **239**(9), 1449 (1967)
36. M.C. Flemings, R. Mehrabian, G.E. Nereo, Trans. TMS-AIME **242**(1), 41 (1968)
37. J. Ni, C. Beckermann, Metall. Trans. B **22B**, 349 (1990)
38. I. Steinbach, Acta Mater. **57**, 2640 (2009)
39. D.V. Alexandrov, A.P. Malygin, Int. J. Heat Mass Transf. **55**, 3196 (2012)
40. A. Subhedar, P.K. Galenko, F. Varnik, Philos. Trans. R. Soc. A **378**, 20190540 (2020)
41. J. Gao, M. Han, A. Kao, K. Pericleous, D.V. Alexandrov, P.K. Galenko, Acta Mater. **103**, 184 (2016)
42. S. He, N. Shevchenko, S. Eckert, IOP Conf. Ser. Mater. Sci. Eng. **861**, 012025 (2020)
43. A. Kao, N. Shevchenko, S. He, P.D. Lee, S. Eckert, K. Pericleous, JOM **72**(10), 3645 (2020)
44. N. Shevchenko, S. Boden, S. Eckert, G. Gerbeth, IOP Conf. Ser. Mater. Sci. Eng. **27**, 012085 (2012)
45. A. Kao, N. Shevchenko, M. Alexandrakis, I. Krastins, S. Eckert, K. Pericleous, Philos. Trans. R. Soc. A **377**, 20180206 (2019)
46. M.T. Rad, C. Beckermann, in *Validation of a Model for the Columnar to Equiaxed Transition with Melt Convection*. CFD Modeling and Simulation in Materials Processing (The Minerals, Metals and Materials Series, Springer, Berlin, 2016), pp. 85–92